Research Square

Preprints are preliminary reports that have not undergone peer review. They should not be considered conclusive, used to inform clinical practice, or referenced by the media as validated information.

Intermediate C=O Formation Is the Bottleneck of Overall Water Splitting on Carbon Nitride

Ji Wu
Jiangsu University
Zhonghuan Liu
Jiangsu University
Xinyu Lin
Jiangsu University
Enhui Jiang
Jiangsu University
Shuai Zhang
Jiangsu University
Pengwei Huo
Jiangsu University
Yan Yan (dgy5212004@163.com)
Jiangsu University
Peng Zhou
Peking University https://orcid.org/0000-0001-8034-8282
Yongsheng Yan
Jiangsu University

Article

Keywords:

Posted Date: May 11th, 2022

DOI: https://doi.org/10.21203/rs.3.rs-1622059/v1

License: This work is licensed under a Creative Commons Attribution 4.0 International License.
Read Full License

Version of Record: A version of this preprint was published at Nature Communications on November 16th, 2022. See the published version at https://doi.org/10.1038/s41467-022-34848-8.

Abstract

Graphitic carbon nitride ($g\text{-}C_3N_4$) was long considered incapable of decomposing pure water molecules into hydrogen and oxygen without the addition of small molecule organics, albeit the superior visible-light response and proper band structure that fulfills the demand of oxygen evolution reaction (OER). Herein, we unexpectedly observed a collective C = O bonding during continuous photocatalytic overall water splitting on single-phased $g\text{-}C_3N_4$ catalyst (denoted CN) by isotopic-labelled ($^{16}O/^{18}O$) *in-situ* diffuse reflection infrared Fourier transform spectroscopy (DRIFTS) and *in-situ* near-ambient pressure X-ray photoelectron spectroscopy (NAP-XPS). Such an inert C = O bonding directly hinders the further OER steps, resulting in a negligible O_2 production on CN. As carbon sites on CN were occupied via the surface fluorination, intermediate C = O bonding was vastly minimized on surface fluorinated CN catalyst (denoted F-CN). As a result, the resulting champion $F_{0.1}$-CN catalyst exhibited excellent overall water splitting activity with the order-of-magnitude improved H_2 evolution rate compared to the pristine CN catalyst and continuous O_2 evolution upon both white light and AM1.5G simulated solar irradiation. Density functional theory (DFT) calculations further suggest an optimized OER pathway on neighboring N atoms by C-F interaction, which effectively avoids the excessively strong C-O interaction or weak N-O interaction on the pristine CN and enhances the stability of formed *OH on the N site of F-CN.

Introduction

Producing hydrogen energy from water splitting using particulate photocatalysts is a low-cost green technology for large-scale solar energy conversion[1–3]. As a two-dimensional metal-free inorganic nanomaterial, graphitic carbon nitride ($g\text{-}C_3N_4$) exhibits superior hydrogen generation ability from water splitting by adding small molecule organics as hole scavengers, with the hydrogen evolution rate under visible-light ($\geq$ 420 nm) even higher than that of the commonly used titanium dioxide catalyst under ultraviolet[4–6]. The overall water splitting has also been achieved on some $g\text{-}C_3N_4$-based composite photocatalysts by constructing in-plane or Z-scheme heterojunctions with oxygen evolution reaction (OER) active cocatalysts[7–9]. However, the single-phased $g\text{-}C_3N_4$ was long considered incapable of photocatalytic overall water splitting due to the insufficient OER ability of $g\text{-}C_3N_4$ to directly produce and release oxygen from pure water[10,11]. Researchers have generally attributed this insufficient OER ability to the weak oxidation capacity of photo-induced valence band holes on $g\text{-}C_3N_4$, thusly assorting $g\text{-}C_3N_4$ as a hydrogen evolution reaction (HER) active only photocatalyst[2,12].

Typically, the one-step excitation overall water splitting requires a semiconductor having a band gap larger than the thermodynamic requirement of 1.23 eV and spanning the redox potential of both HER and OER[13,14]. However, with an energy band gap greater than 2.0 eV and the positions of both valence and conduction bands that fully meet the thermodynamic demands of water[15,16], single-phased pristine $g\text{-}C_3N_4$ catalysts still failed to directly extract O_2 from pure water, indicating that unknown factors rather than the high valence band position hinders the OER on $g\text{-}C_3N_4$. For single-phased $g\text{-}C_3N_4$, figuring out the bottleneck that hinders the OER and how to bypass such a bottleneck to achieve efficient overall water splitting under visible light is of utmost importance.

Herein, by *in-situ* observations using isotopic-labelled ($^{16}O/^{18}O$) diffuse reflection infrared Fourier transform spectroscopy (DRIFTS) and near-ambient pressure X-ray photoelectron spectroscopy (NAP-XPS), we confirmed that the strong C = O bonding at $H_2O/g\text{-}C_3N_4$ interface as an inert intermediate state directly hinders the subsequent OER, which is the bottleneck to prevent the continuous overall water splitting on the single-phase pristine $g\text{-}C_3N_4$ catalyst. Preventing the C = O formation via a simple surface fluorination strategy restored deserved overall water splitting activity on fluorinated $g\text{-}C_3N_4$ catalysts with the champion H_2 evolution rate was order-of-magnitude improved compared to the pristine CN and continuous O_2 evolution upon both white light and AM1.5G simulated solar irradiation. Density functional theory (DFT) calculations were further employed to simulate the surface fluorination-promoted OER at H_2O/CN interface and evaluate the impact of different intermediate OER configurations.

Results And Discussion

Typical $g\text{-}C_3N_4$ catalyst (denoted CN) was prepared by sintering melamine powder at 550°C in a muffle furnace according to a classic protocol from literature (for details of the preparation method, see Supplementary Information)[17]. We first used isotopic $^{16}O/^{18}O$ labelled H_2O for *in-situ* tracing of possible OER intermediate at the H_2O/CN interface during continuous reaction by DRIFTS. H_2O molecules were carried into the reaction chamber by N_2 flow until equilibrium. Setting the equilibrium condition as the blank background, positive or negative IR response signal directly reflects the gain or loss of intermediate species at H_2O/catalyst interface. As shown in Fig. 1a, when the CN/H_2O sample was used and irradiated *in situ* with a 420 nm LED lamp, a broad negative absorption band from 3700 cm^{-1} to 3000 cm^{-1} and a very weak negative peak at 1645 cm^{-1} emerged from the background and increased in intensity with increasing irradiation time. The broad negative band was assigned to the stretching vibration of O-H bond, whereas the weak negative peak at 1645 cm^{-1} was from the bending vibration of H-O-H of H_2O molecules, representing the loss of surface -OH species and H_2O molecules during continuous OER[18,19]. The signal of O-H stretching vibration was much larger than the bending vibration signal of H_2O molecules, suggesting that the OER occurred at H_2O/CN interface was predominantly in the form of dissociated O-H. Identical features were observed when CN was replaced with other CN sample (i.e., $F_{0.1}$-CN), or when H_2O was replaced with ^{18}O-labelled $H_2{}^{18}O$ (Fig. 1a-1d) as the signature of OER at the H_2O/CN interface. More importantly, an increasing positive peak at 1725 cm^{-1} that ascribed to the C = O stretching vibration was observed with increasing irradiation time (Fig. 1a), indicating that the collective formation of C = O species on CN surface. When we replaced H_2O with ^{18}O-labelled $H_2{}^{18}O$ under otherwise identical conditions (Fig. 1b), the positive peak at 1725 cm^{-1} and the newly generated peak at 1524 cm^{-1} emerged in terms of the theoretical $^{16}O/^{18}O$ replacement effect, which confirms that the O source of C = O was from H_2O and further provides direct evidence for C = O formation during photocatalytic OER at H_2O/CN interface. Such a C = O formation can only occur with carbon sites on CN being oxidized. To prevent the formation of C = O on CN, we devised a surface fluorination strategy to occupy carbon-sites on CN with F^- ions through a hydrothermal treatment. Prepared fluorinated CN samples (denoted F-CN) were labeled as $F_{0.01}$-CN ~ F_1-CN with different F^- concentration (0.01 mM ~ 1 mM) of the precursor for fluorination (for details of the preparation method, see Supplementary Information). The surface fluorination did not severely change the morphology (Supplementary Fig. 1) and crystalline structure of CN (Supplementary Fig. 2), but formed a strong C-F interaction (Supplementary Fig. 3). When we replaced CN with $F_{0.1}$-CN (Fig. 1c), the positive C = O signal was no longer observed at the $H_2O/F_{0.1}$-CN interface. Further replacing the H_2O with ^{18}O-labelled $H_2{}^{18}O$ under otherwise identical conditions showed neither C = O nor C = ^{18}O diagnostic signals (Fig. 1d), which solidly confirms that the fluorination of CN prevents the carbon sites being oxidized into C = O intermediates.

The collective formation of C = O state by oxidizing carbon sites on CN was also directly observed by NAP-XPS. The NAP-XPS spectra were *in-situ* collected in a vacuum chamber with 0.2 mbar H_2O vapor pressure. A 300 W Xenon lamp as the white light source was placed outside the chamber to illuminate the sample via the quartz window. On the O1s spectra of the pristine CN sample, two major peaks at 530.1 eV and 531.3 eV were observed, corresponding to oxygen states of C-O and O-H species (Fig. 1e**)**, respectively[20]. Under the white light illumination, a newly emerged contribution at 532.7 eV from C = O configuration was observed and increased in intensity with increasing irradiation time (Fig. 1e). Moreover, on the C1s spectra, peaks of C-C and N = C-N states on the pristine CN were gradually shifted towards higher binding energy from 284.4 eV and 287.7 eV to 284.9 eV and 288.1 eV (Supplementary Fig. 4a), respectively, under continuous white light illumination, corresponding to the formation of an oxidized carbon state on CN[21]. The NAP-XPS result is consistent with *in-situ* DRIFTS observations (Fig. 1a,b), demonstrating that C = O intermediate state was indeed formed at the H_2O/CN interface during OER. After fluorination, although the strong C-F interaction can be recognized from the C1s peak shifting of $F_{0.1}$-CN sample in comparison with CN (Supplementary Fig. 3a), little changes were found on both O1s (Fig. 1f) and C1s Supplementary Fig. 4b) spectra of $F_{0.1}$-CN during continuous white light illumination with 0.2 mbar H_2O vapor, which further demonstrates that C = O formation was vastly minimized on F-CN. In contrast, no changes were found on the N1s spectra on both CN and $F_{0.1}$-CN samples (Supplementary Fig. 4c,d).

We argue that the strong C = O bonding from carbon site oxidation is an inherent bottleneck for OER on single-phased CN catalysts. If that is the case, preventing the intermediate C = O formation would endow CN catalysts deserved overall water splitting performances. Photocatalytic overall water splitting experiments on CN and different F-CN samples were performed in pure water without any organic sacrificial reagents under both the white light (Fig. 2a) and AM1.5G simulated solar irradiation (Fig. 2b). Under continuous white light irradiation (Xe lamb, 1000 mW cm^{-2}), the pristine CN catalyst only exhibited a mild H_2 evolution of 11.60 μmol•g^{-1}•h^{-1} without O_2 evolution. After hydrothermal treatment, CN exfoliated thin layer sample (denoted CN-E) showed a slightly higher H_2 evolution rate of 20.22 μmol•g^-

^{1}•h^{-1} due to the enlarged specific surface area of CN-E (62.12 m^2•g^{-1}) in comparison with CN (8.66 m^2•g^{-1}), but still no O_2 evolution observed. The poor performance on CN and CN-E catalysts is consistent with literature reports[22,23], demonstrating that single-phased g-C_3N_4 catalyst dose not possess the overall water splitting ability. However, after the fluorination treatment, all F-CN catalysts exhibited both H_2 and O_2 evolution capabilities under identical experimental conditions, which varies with the fluorination degree. Particularly, the champion $F_{0.1}$-CN catalyst exhibited the H_2 evolution rate of 174.77 μmol•g^{-1}•h^{-1}, which is 15.06 and 8.64 times higher than those of the pristine CN and CN-E catalysts, respectively, and continuous O_2 evolution of 44.15 μmol•g^{-1}•h^{-1} (Fig. 2a). Although the specific surface area of $F_{0.1}$-CN (42.69 m^2•g^{-1}) is larger than that of the pristine CN (8.66 m^2•g^{-1}) after hydrothermal exfoliation treatment, it is still smaller than that of CN-E (62.12 m^2•g^{-1}) (Supplementary Fig. 5), yet $F_{0.1}$-CN exhibited an order-of-magnitude-improved water splitting efficiency (Fig. 2a,b). Further increase the F^- ions would slightly decrease the performance of as-prepared F-CN catalysts, which is attributed to the enhanced hydrophobic feature by fluorination (Supplementary Fig. 6). Moreover, under AM1.5 simulated solar irradiation, the $F_{0.1}$-CN catalyst still exhibited excellent overall water splitting capacity with H_2 evolution rate of 83.89 μmol•g^{-1}•h^{-1}, increasing by 9.63 times in comparison with the pristine CN catalyst (8.71 μmol•g^{-1}•h^{-1}), and continuous O_2 evolution rate of 21.15 μmol•g^{-1}•h^{-1}. Control experiments have been done to confirm no H_2/O_2 productions were detected in the dark, no catalysts or without H_2O for the $F_{0.1}$-CN catalyst (Supplementary Fig. 7). Isotopic labeled experiments also confirmed that H_2 and O_2 were produced sorely from the photocatalytic water splitting rather than other effects, whereas D_2 and $^{18}O_2$ were detected as products of D_2O and ^{18}O-labelled $H_2{}^{18}O$ (Supplementary Fig. 8). Notably, H_2/O_2 production ratio on F-CN catalysts was less than the stoichiometric ratio of 2:1 (Fig. 2a,b). The short of O_2 production on F-CN was due to the further reduction of O_2 into H_2O_2, since CN is very active for O_2 reduction[24,25], which was further demonstrated by the *in-situ* observation of H_2O_2 production during the reaction (Supplementary Fig. 9) by the well-reported Ghormley triiodide method[26]. Furthermore, within 20 hours, $F_{0.1}$-CN can still maintain more than 80% of efficiency on H_2 and O_2 production and continue to work, in contrast, CN and CN-E were quickly deactivated with less than 50% of initial efficiency on H_2 production within 8 hours (Supplementary Fig. 10), indicating that the H_2 evolution on $F_{0.1}$-CN came from the continuous overall water splitting, whereas the mild H_2 evolution on CN and CN-E was possibly from the unsustainable self-oxidation.

Comparing above photocatalytic performance results with our *in-situ* DRIFTS (Fig. 1a-1d) and *in-situ* NAP-XPS (Fig. 1e,f) observations, we reason that the intermediate C = O formation is the bottleneck of overall water splitting on single-phased CN catalysts. To further verify that the emerging overall water splitting ability on F-CN is due to the preventing of C = O formation rather than other effects, we first compared the visible-light absorption of CN and F-CN catalysts. Figure 2c shows the wavelength dependence of apparent quantum yield (AQY) on the pristine CN and the champion $F_{0.1}$-CN catalysts along with the ultraviolet-visible diffuse reflection spectra (UV-vis DRS). As peak values, AQYs at 365 nm on both samples were determined to be 0.5718% ($F_{0.1}$-CN) and 0.1281% (CN). When the incident wavelength increased from 365 nm to 500 nm, AQYs of both samples were sharply decreased (Supplementary Table 1 and Table 2), which coincides with literature reports on g-C_3N_4-based catalysts[27,28]. In visible-light region, AQYs at 420 nm on both samples were determined to be 0.0164% ($F_{0.1}$-CN) and 0.0005% (CN). The much higher AQYs on $F_{0.1}$-CN catalyst than that on the pristine CN catalyst further evince the effect of fluorination treatment. However, from UV-vis DRS spectra, no discernible differences on the absorption edge between CN and $F_{0.1}$-CN were observed, indicating that the improved overall water splitting performance of F-CN was not from the enhanced visible-light response.

We further tracked the transient fluorescence emission profile at 465 nm on both $F_{0.1}$-CN and CN catalysts with the incident 375 nm irradiation and found that the emission lifetime of the $F_{0.1}$-CN catalyst is not significantly extended in comparison with the pristine CN catalyst (Fig. 2d). The fitted emission decay profiles suggest a slightly shortened exciton lifetime on $F_{0.1}$-CN with lifetime parameter reduced from τ_A = 7.72 ns to τ_A = 6.36 ns in comparison with the pristine CN, which denies the extended exciton lifetime as the major effect of fluorination for enhanced overall water splitting performances. Moreover, from the XPS valence band (VB) spectra near Fermi level (Supplementary Fig. 11), both CN and $F_{0.1}$-CN exhibited almost identical VB position at 1.88 eV, which denies the VB position as the major contributor for the order-of-magnitude performance improvement on F-CN.

Through above characterizations, we ruled out that the morphology, crystalline structure, visible-light response, exciton lifetimes, and VB positions are the main factors affecting the performance of F-CN for overall water splitting. However, by using *in-situ* DRIFTS (Fig. 1a-1d) and NAP-XPS (Fig. 1e,f, Supplementary Fig. 4), we successfully identified the formation of C = O intermediate and their minimization on F-CN surface, which is completely consistent with the tendency of photocatalytic water splitting performances. Therefore, we conclude that the formation of C = O intermediate is an important bottleneck for overall water splitting on single-phased CN catalyst. By occupying the carbon site on CN surface by fluorination, this bottleneck can be bypassed to achieve efficient visible-light-driven H_2 and O_2 productions from overall water splitting on single-phased F-CN catalysts.

DFT calculations were further employed to investigate the effect of surface flurination on the water decomposition reaction (i.e., OER) on CN/F-CN surface (for details of the computational methods, see Supplementary Information). F-CN layer was formed by using one F atom to bond with the C atom in CN (Supplementary Fig. 12). Water adsorption and activation were simulated on both C sites (Fig. 3a) and N sites (Supplementary Fig. 13a) in pristine CN and N atoms adjacent to the C-F bond in F-CN as reactive sites (Fig. 3b). Calculated free energy profiles show that OER on surface C site has a lower energy barrier (2.25 eV) than the surface N site (2.86 eV) in CN (Fig. 3c), indicating that C site is the predominant OER reactive sites in the pristine CN. Moreover, after F atom ocupying the C site, the surface N site in F-CN owns a much lower energy barrier (1.58 eV) than the surface C (2.25 eV) or N (2.86 eV) site in pristine CN (Fig. 3c), demonstrating that the F modification indeed can improve the OER activity on F-CN. According to the corresponding evolution pathway of geometry structures (Fig. 3a,b), the improved OER activity is considered due to the C-F bond formation optimizing the OER pathway on adjacent N atoms. Especially, the calculated charge density difference mappings show that the F modification in F-CN optimizes the bonding interaction between CN surface and *OH intermediate (Fig. 3e), which effectively avoids the excessively strong C-O interaction (Fig. 3d) or weak N-O interaction (Supplementary Fig. 13b) in pristine CN. As a result, the F modification greatly decreases the formation energy of rate-determining *OH. It should be noted that the F modification also significantly promote the formation of *OOH, which is also a high-barrier reaction step in OER (Fig. 3c). This implies that the excessively stable *O intermediate in the form of C = O bond on pristine CN is difficult to be further converted into *OOH. As a result, CN with an observable IR signal of C = O during reaction owns a lower activity than F-CN, which completely coincides with our experimental observations. Furthermore, the PDOS reveals that the different bonding behavior between *OH and catalyst surface is attributed to the F modification that enables the N2p states to move upward the Fermi level (Fig. 3f), which effectively enhances the stability of formed *OH on the N site in F-CN. Thus, the N site in F-CN is the main OER center.

Conclusion

The unexpected C = O formation by oxidizing surface carbon atoms during the OER on single-phased CN catalysts is a previously unrecognized event. Such a strong bonding of intermediate C = O would no doubt significantly hinder the further OER steps as the bottleneck of overall water splitting on CN-based catalysts. Our present study is the first to identify the unrevealed cause that is responsible for overall water splitting inactivation on single-phased CN catalysts. To bypass this bottleneck, a simple and robust surface fluorination treatment to suppress C = O bonding by forming C-F was devised, which significantly restores the deserved overall water splitting ability under visible-light on resulting F-CN catalysts.

Declarations

Acknowledgement

We are grateful for the technical support from Dr. Yifan Li and Prof. Yi Cui of Nano-X from Suzhou Institute of Nano-Tech and Nano-Bionics, Chinese Academy of Sciences (SINANO). We gratefully acknowledge the financial support of the National Natural Science Foundation of China (Grant No. 21776117 and 21806060).

Author contribution list

J. Wu and Y. Yan designed the whole experiments. J. Wu, Z. Liu, X. Lin, E. Jiang and S. Zhang conducted most experiments. J. Wu and Y. Yan wrote the paper. P. Zhou contributed to the DFT calculation. P. Huo, P. Zhou and Y.S. Yan contributed to the data analysis the paper quality by discussions.

References

1. Chen, S., Takata, T. & Domen, K. Particulate photocatalysts for overall water splitting. Nat. Rev. Mater. **2**(2017).
2. Wang, Q. & Domen, K. Particulate Photocatalysts for Light-Driven Water Splitting: Mechanisms, Challenges, and Design Strategies. Chem. Rev. **120**, 919–985 (2020).
3. Green, M.A. & Bremner, S.P. Energy conversion approaches and materials for high-efficiency photovoltaics. Nat. Mater. **16**, 23–34 (2016).
4. Wang, X. et al. A metal-free polymeric photocatalyst for hydrogen production from water under visible light. Nat. Mater. **8**, 76–80 (2009).
5. Zhou, G. et al. Half-metallic carbon nitride nanosheets with micro grid mode resonance structure for efficient photocatalytic hydrogen evolution. Nat. Commun. **9**, 3366 (2018).
6. Yu, S. et al. Local spatial charge separation and proton activation induced by surface hydroxylation promoting photocatalytic hydrogen evolution of polymeric carbon nitride. Nano. Energy. **50**, 383–392 (2018).
7. Che, W. et al. Fast Photoelectron Transfer in (C_{ring})-C_3N_4 Plane Heterostructural Nanosheets for Overall Water Splitting. J. Am. Chem. Soc. **139**, 3021–3026 (2017).
8. Chen, X., Wang, J., Chai, Y., Zhang, Z. & Zhu, Y. Efficient Photocatalytic Overall Water Splitting Induced by the Giant Internal Electric Field of a g-C_3N_4 /rGO/PDIP Z-Scheme Heterojunction. Adv. Mater. **33**, e2007479 (2021).
9. Zhao, D. et al. Boron-doped nitrogen-deficient carbon nitride-based Z-scheme heterostructures for photocatalytic overall water splitting. Nat. Energy **6**, 388–397 (2021).
10. Liu, J. et al. Water splitting. Metal-free efficient photocatalyst for stable visible water splitting via a two-electron pathway. Science **347**, 970–974 (2015).
11. Zhang, G., Lan, Z.A. & Wang, X. Surface engineering of graphitic carbon nitride polymers with cocatalysts for photocatalytic overall water splitting. Chem. sci. **8**, 5261–5274 (2017).
12. Butchosa, C., Guiglion, P. & Zwijnenburg, M.A. Carbon Nitride Photocatalysts for Water Splitting: A Computational Perspective. J. Phys. Chem. C. **118**, 24833–24842 (2014).
13. Wang, Z., Li, C. & Domen, K. Recent developments in heterogeneous photocatalysts for solar-driven overall water splitting. Chem. Soc. Rev. **48**, 2109–2125 (2019).
14. Jafari, T. et al. Photocatalytic Water Splitting-The Untamed Dream: A Review of Recent Advances. Molecules **21**(2016).
15. Zhao, C., Chen, Z., Shi, R., Yang, X. & Zhang, T. Recent Advances in Conjugated Polymers for Visible-Light-Driven Water Splitting. Adv. Mater. **32**, e1907296 (2020).
16. Eliseeva, S. V & Bünzli, J.-C. G. Rare earths: jewels for functional materials of the future. New Journal of Chemistry **35**, (2011).
17. Wang, Y., Wang, X. & Antonietti, M. Polymeric graphitic carbon nitride as a heterogeneous organocatalyst: from photochemistry to multipurpose catalysis to sustainable chemistry. Angew. Chem. Int. Ed. **51**, 68–89 (2012).

18. Sheng, H. et al. Activation of Water in Titanium Dioxide Photocatalysis by Formation of Surface Hydrogen Bonds: An In Situ IR Spectroscopy Study. Angew. Chem. Int. Ed. **54**, 5905–9 (2015).
19. Yan, Y. et al. Proton-free electron-trapping feature of titanium dioxide nanoparticles without the characteristic blue color. Commun. Chem. **2**(2019).
20. Chen, X. et al. Three-dimensional porous g-C_3N_4 for highly efficient photocatalytic overall water splitting. Nano Energy **59**, 644–650 (2019).
21. Jin, Z. et al. Infrared response in photocatalytic polymeric carbon nitride for water splitting via an upconversion mechanism. Commun. Mater. **1**(2020).
22. Liu, H. et al. Linking melem with conjugated Schiff-base bonds to boost photocatalytic efficiency of carbon nitride for overall water splitting. Nanoscale **13**, 9315–9321 (2021).
23. Liu, W. et al. Single-Site Active Cobalt-Based Photocatalyst with a Long Carrier Lifetime for Spontaneous Overall Water Splitting. Angew. Chem. Int. Ed. **56**, 9312–9317 (2017).
24. Zhao, Y. et al. Mechanistic analysis of multiple processes controlling solar-driven H_2O_2 synthesis using engineered polymeric carbon nitride. Nat. Commun. **2**, 3701 (2021).
25. Wu, S., Yu, H., Chen, S. & Quan, X. Enhanced Photocatalytic H2O2 Production over Carbon Nitride by Doping and Defect Engineering. ACS Catal. **10**, 14380–14389 (2020).
26. Diesen, V. & Jonsson, M. Formation of H_2O_2 in TiO_2 Photocatalysis of Oxygenated and Deoxygenated Aqueous Systems: A Probe for Photocatalytically Produced Hydroxyl Radicals. J. Phys. Chem. C. **118**, 10083–10087 (2014).
27. Lin, L. et al. Molecular-level insights on the reactive facet of carbon nitride single crystals photocatalysing overall water splitting. Nat. Catal. **3**, 649–655 (2020).
28. Lin, Y., Su, W., Wang, X., Fu, X. & Wang, X. LaOCl-Coupled Polymeric Carbon Nitride for Overall Water Splitting through a One-Photon Excitation Pathway. Angew. Chem. Int. Ed. **59**, 20919–20923 (2020).

Figures

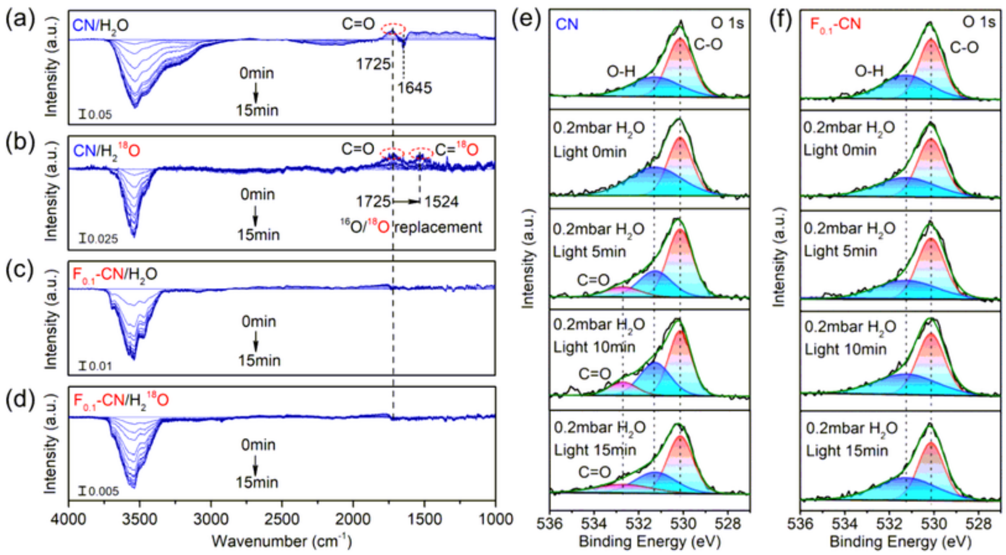

Figure 1

DRIFTS spectra *in-situ* monitored at **(a)** CN/H_2O, **(b)** CN/$H_2{}^{18}O$, **(c)** $F_{0.1}$-CN/ H_2O and **(d)** $F_{0.1}$-CN/ $H_2{}^{18}O$ interface under constant 420 nm (3W, LED) irradiation in 15 min using pristine CN and the champion fluorinated F-CN ($F_{0.1}$-CN) catalysts. **(e)** *In-situ* NAP-XPS O1s spectra on pristine CN and **(f)** $F_{0.1}$-CN catalysts with 0.2 mbar H_2O vapor pressure using a 300 W Xenon lamp as the white light source in 15 min.

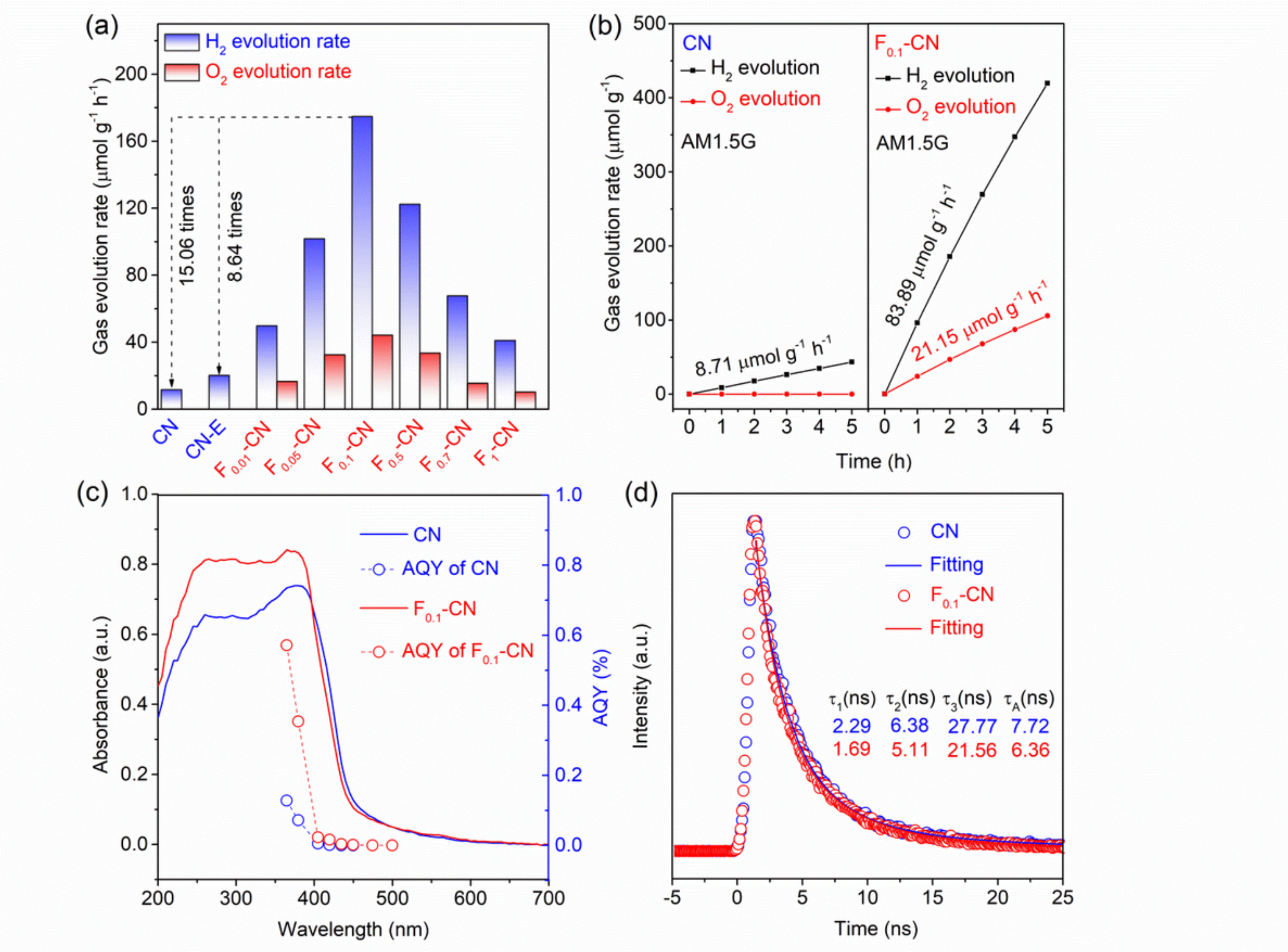

Figure 2

(a) Photocatalytic H_2 and O_2 productions from pure water on pristine CN, CN-E and different F-CN catalysts under white light illumination. **(b)** Time-profiles of photocatalytic H_2 and O_2 productions from pure water on pristine CN and $F_{0.1}$-CN under AM 1.5G simulated solar irradiation. **(c)** Wavelength-dependent AQYs on pristine CN and $F_{0.1}$-CN along with the corresponding UV-vis DRS spectra. **(d)** Transient fluorescence emission decay at 465 nm on CN and $F_{0.1}$-CN catalysts with 375 nm excitation.

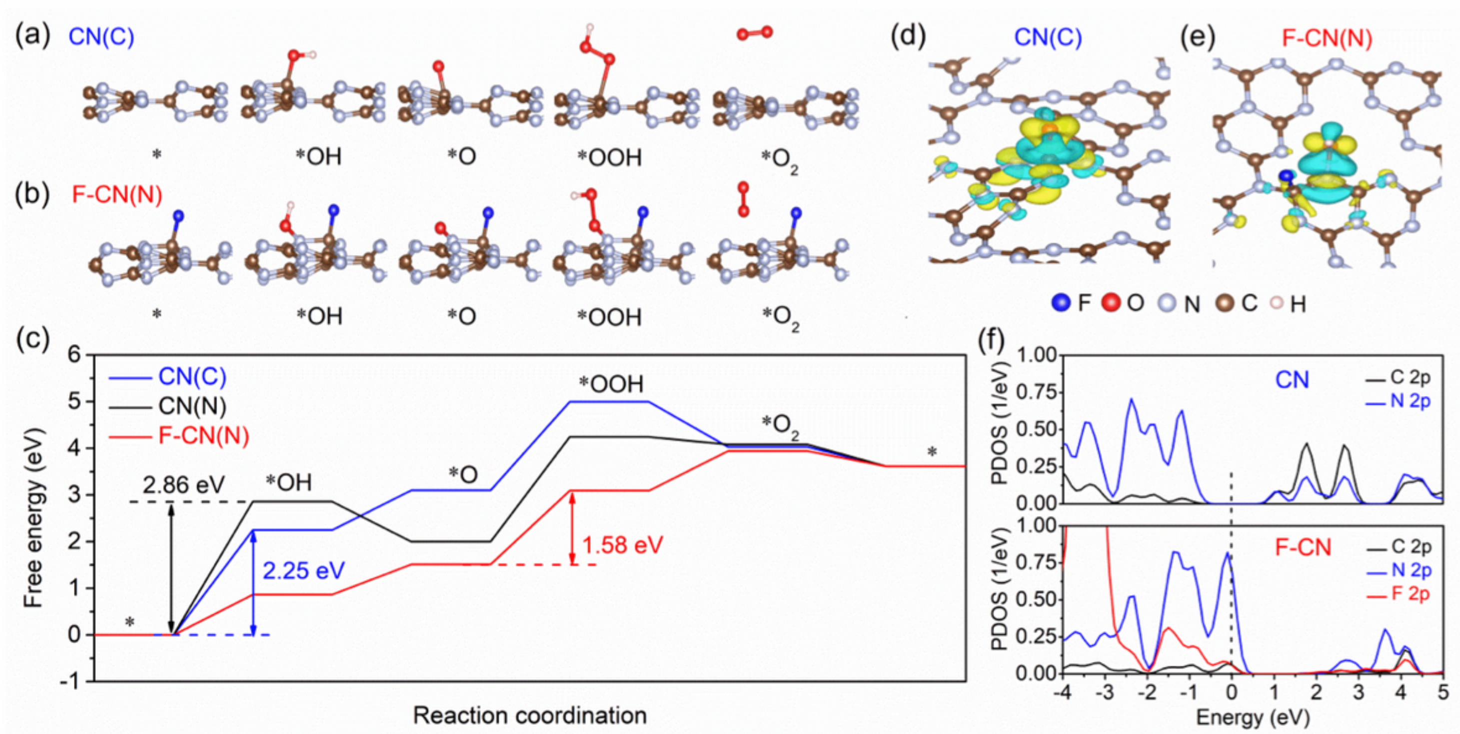

Figure 3

Water adsorption and activation were simulated on **(a)** on C site in pristine CN (denoted CN(C)) and **(b)** on N site in F-CN (denoted F-CN(N)). **(c)** Free energy profiles of OER on CN and F-CN at pH = 7 and U = 0 V *vs* SHE (where * represents the intermediate state). CN(C) represents C reaction sites on the pristine CN; CN(N) represents N reaction sites on the pristine CN; F-CN (N) represents N reaction sites on F-CN (C reaction sites occupied entirely by F atoms). Charge density difference mappings between *OH intermediate and catalyst surface: **(d)** CN(C) and **(e)** F-CN(N). The blue and yellow isosurfaces stand for the negative and positive charges, respectively. The isosurface of charge density is set to 0.005 e $Å^{-3}$. **(f)** PDOS of 2p states of surface C, N and F in CN and F-CN. The dashed line stands for Fermi level.

Supplementary Files

This is a list of supplementary files associated with this preprint. Click to download.

- SupplementaryInformationWJ.docx